13th ewtec 2019 Proceedings of the 13th European Wave and Tidal Energy Conference 1-6 Sept 2019, Naples, Italy

Model performance predicting extreme wave heights for project risk assessment and WEC design

Vincent S. Neary, Bibiana Seng, Zhaoqing Yang, Nabi Allahdadi, Ruoying He, and Taiping Wang

Abstract— **The model skill predicting extreme significant wave heights at 50, 5, and 1-year recurrence intervals is evaluated at buoy locations within several regional wave climates along the US East and West Coasts. Two common third-generation spectral wave models are evaluated, a WAVEWATCH III® (WWIII) model with a grid resolution of 4 minutes, and a Simulating WAves Nearshore (SWAN) model, with a resolution of 200-300 m. Both models are used to generate multi-year hindcasts from which sea state statistics used for wave conditions characterization and classification can be derived and compared to those derived from in situ observations made at National Data Buoy Center (NDBC) stations. Our comparisons generally show underbias for extreme wave heights derived from model hindcasts. This underbias is significantly larger for wave heights derived from WWIII hindcasts than those derived from SWAN hindcasts, primarily due to the coarser resolution of the WWIII model. However, simple linear corrections to compensate for this bias can be applied to improve results that are satisfactory for assessing wave energy project risk and wave energy converter (WEC) design.**

Keywords—**extreme wave height, wave hindcast, wave energy resource assessment, WEC design.**

I. Introduction

EXTREME sea state statistics, like the 50-year return period significant wave height, $H_{s(50)}$, are key metrics used to characterize extreme wave conditions for a host of ocean (offshore) and coastal engineering applications [1], including offshore wind and marine energy. In marine energy, the significant wave height recurring every 50-years on average, $H_{s(50)}$, has been proposed as an indicator of project risk using a relative risk ratio, $H_{s(50)}/H_{s(mean)}$ [2], [3]. In addition, the International Electrotechnical Commission (IEC) is developing a design standard for wave energy converters (WEC) that requires $H_{s(50)}$ for building extreme design wave load cases [4].

Muir and El-Shaarawi [5] review data sources and their limitations for calculating n-year significant wave height statistics: Wave buoys are known to underestimate very large individual waves, e.g., [6]; spatial coverage is limited beyond the point of observation; and measurement durations are typically insufficient to calculate extreme sea state statistics [1]. Wave buoys, however, provide reliable point observations of extreme significant wave height, [6], and are the primary data source for ground-truthing wave models.

Spectral wave model hindcasts, using models like WAVEWATCH III® (WWIII) and Simulating WAves Nearshore (SWAN), are an alternative data source for estimating extreme wave height statistics, and accepted for wave energy resource assessment and ocean engineering design when validated with buoy measurements [7], [8]. Model hindcasts also provide a means to address the noted limitations of spatial coverage and measurement duration from buoy observations.

Model performance studies have demonstrated that the third-generation spectral wave models WWIII and SWAN can accurately predict a host of wave energy resource statistics, and that their accuracy is significantly improved with grid refinement [9], [10]. Further, these models can examine the spatial variation of wave characteristics at fine resolutions over larger regions encompassing different wave climates, e.g., [11]. These models, however, underpredict large waves and extreme n-year significant wave heights. The main source of this underbias is due to limitations of most wind reanalysis datasets, namely their inability to resolve fine-scale high-energy wind gusts, e.g., [12], [13].

Paper ID number: 1347- Conference track: WRC

V. S. Neary (corresponding author) is with Water Power Technologies, Sandia National Laboratories, PO Box 5800, Albuquerque, NM 87185 USA (e-mail: vsneary@sandia.gov).

B. Seng is with Water Power Technologies, Sandia National Laboratories, PO Box 5800, Albuquerque, NM 87185 USA. (e-mail: beseng@sandia.gov)

Z. Yang is with Marine Sciences Laboratory, 1100 Dexter Ave North, Suite 500, Seattle, WA 98109 USA (e-mail: zhaoqing.yang@pnnl.gov).

N. Allahdadi is with Dept. Marine, Earth and Atmospheric Sciences, North Carolina State University, Raleigh, NC 27695 USA (e-mail: mallahd@ncsu.edu).

Ruoying He is with Dept. Marine, Earth and Atmospheric Sciences, North Carolina State University, Raleigh, NC 27695 USA (e-mail: rhe@ncsu.edu).

Taiping Wang is with Marine Sciences Laboratory, 1100 Dexter Ave North, Suite 500, Seattle, WA 98109 USA (e-mail: taiping.wang@pnnl.gov).

 Copyright © European Tidal and Wave Energy Conference 2019

Numerous studies have investigated wave model performance using buoy observations as ground truth. Such studies commonly emphasize predictions of common sea state statistics (bulk parameters) on average, e.g., H_s and peak period, T_p; comparing these statistics with those derived from buoy observations at some regular time interval. Few studies have evaluated model performance predicting extreme wave heights. Yang et al. [9] observed significant prediction underbias of large waves occurring during historic storm events. Stephens and Gorman [14] showed significant underprediction of $H_{s(100)}$ by the WAM model for large values at sites around New Zealand.

The present study evaluates model skill predicting extreme significant wave heights with 50, 5 and 1-year recurrence intervals, $H_{s(50)}$, $H_{s(5)}$, and $H_{s(1)}$, at approximately two dozen buoy locations spanning several regional wave climates along the US East and West Coasts. It also investigates simple linear corrections to modelled extreme wave heights to improve results. While this model performance evaluation does not consider spectral details that can identify sources of model deficiencies, e.g., [15], it does provide an initial assessment of model performance trends, including bias, and how performance may vary among different wave climates.

II. METHODS

Two spectral wave models are evaluated, a WWIII model with a spatial resolution of 4-minutes [16], and a SWAN model employed for two high-resolution regional model hindcasts for wave energy resource characterization and classification [17], one for the US East Coast [10] and one for the US West Coast [10]; each with a grid resolution of 200-300 m in the study region. Hourly H_s time series output from these model hindcasts are used to estimate $H_{s(50)}$, $H_{s(5)}$, and $H_{s(1)}$ for comparison with those derived from measured (observation) H_s time series at National Data Buoy Center (NDBC) stations at eight sites along the East Coast and thirteen sites along the West Coast.

The study region, shown in Fig. 1, encompasses potential wave energy project sites within the economic exclusion zones along the eastern and western coastlines of the US. Only NDBC stations with long deployment periods of at least 15 years are selected, but missing data records reduced useful periods of record for some sites below this threshold to just 10 years (Fig. 1, Table I). Depths at these buoy sites vary from 30 m (44009) to 4,048 m (41002) and are classified as intermediate and deep wave sites with normalized peak frequencies of $f_P > 0.05\sqrt{g/h}$.

The annual maxima method is used to estimate $H_{s(50)}$ and $H_{s(5)}$ from H_s time series generated from models and buoy observations for comparison, with hourly values from all data sources at corresponding intervals and spanning the same period of record (POR) to ensure consistency. This method, which fits the yearly maxima H_s to a Gumbel distribution, is an accepted standard [8], simple to implement, and requires no user inputs like peak-over-threshold (POT) methods that can introduce user bias. It does, however, require a minimum POR of approximately 20-years [18]. While this requirement is not met for ten sites, H_s data from these sites still exceeds 10-years and strengthens the correlation between the model and measurement derived $H_{s(n)}$ by doubling the population of samples. As the same POR is used for model and measurement derived data sources, the bias introduced by relaxing this requirement is consistent for both data sources.

For very low recurrence intervals, below 5-years, POT methods are recommended [1]. We apply the *MQQR* POT method described in [18] to estimate $H_{s(1)}$. This method uses quantile-quantile (QQ) plots to ensure data fits the modelled distributions, and the Wald-Wolfowitz Runs (WWR) test to ensure samples are independent.

A simple linear correction method proposed by Stephens and Gorman [14] is applied to improve the agreement between $H_{s(n)}$ values derived from modelled and measured (observation) data sources, where modelled $H_{s(n)}$ values are scaled by the average relative bias among the study sites,

$$s = \frac{1}{N}\sum_{i=1}^{N}\frac{Mod.H_{s(n),i} - Obs.H_{s(n),i}}{Mod.H_{s(n),i}} \quad (1)$$

where N is the number of sites, and i is the site index. This correction scaling constant, s, should not be confused with the average mean bias that considers bias relative to the measurement-derived value to evaluate the model performance.

To compare the goodness of fit between the model and measurement-derived $H_{s(n)}$ values, a linear regression best-fit line is plotted along with the line of equivalence, and r^2, slope (m) and y-intercept (b) values are reported (Fig. 2-4). The mean absolute relative bias (B) is calculated as a summary statistic to quantify this comparison,

$$B = \frac{1}{N}\sum_{i=1}^{N}\left|\frac{Mod.H_{s(n),i} - Obs.H_{s(n),i}}{Obs.H_{s(n),i}}\right| \quad (2)$$

Here, the bias is relative to the measured data source (observation) rather than the modelled data source as calculated for the scaling factor calculated using (1).

III. RESULTS

Results of our comparison between model and measurement-derived $H_{s(50)}$, $H_{s(5)}$, and $H_{s(1)}$ values are summarized in Tables I-III, and visualized in scatter plots in Figs. 2-4. Raw, uncorrected, and corrected $H_{s(n)}$ derived by model hindcasts are given for each site with percent relative bias in parentheses. With the exception of $H_{s(n)}$ derived from SWAN hindcasts for buoys 46054 and 46026, and $H_{s(50)}$ derived from SWAN hindcasts for buoy 41004, the raw values of $H_{s(n)}$ derived from both models, as shown in Figs. 2-4 (a, c) and Tables 1-3, are lower than

those derived from buoy observations. This model underbias among all $H_{s(n)}$ is more pronounced for WWIII, which has an average model relative absolute bias of approximately 20%, compared to approximately 10% for SWAN. Correlations of linear regression fits shown in Figs. 2-4 (a, c) did not improve by separating the study sites by regional wave climate (East Coast, West Coast).

Corrections applied to the model-derived $H_{s(n)}$ with the scaling factors calculated using (1) significantly improve the agreement between model and measurement-derived values. The average relative absolute bias for WWIII is reduced to 3-4%, and that for SWAN to 6-7%. Comparing scatter plots, Figs. 2-4 (a, b) for WWIII, and Figs. 2-4 (c, d) for SWAN, illustrates how this simple correction adjusts values to better align with the line of equivalence. Slopes, m, and y-intercepts (b) of linear regression fits for $H_{s(50)}$ quantify these improvements; Best fit slopes show corrections change m=0.76 to 0.99 for WWIII plots, and m=0.84 to 0.91 for the SWAN plots; while y-intercepts, b, increase, but only slightly.

Comparison of raw and corrected $H_{s(50)}$ esimates for all 1,978 WWIII modelled sites are shown in Figs. 5 (a,c), and those for $H_{s(50)}/H_{s(mean)}$ are shown in Fig. 5 (b,d), to illustrate the importance of correcting model bias for the purpose of wave energy resource assessment and WEC design.

IV. Conclusion

The present study shows that validated model hindcasts underpredict extreme significant wave height with 50, 5 and 1-year recurrence intervals, which corroborates with past studies showing model underprediction of $H_{s(100)}$, e.g., [14], and model underprediction for large H_s occurring in episodic storm events when large wind gusts occur, e.g., [9].

Applications of grid refinement and improved model physics and atmospheric forcing data can significantly reduce model bias predicting extreme wave heights. However, simple linear correction methods may offer a more economical approach to offset this observed model bias. Additional efforts are needed to more rigorously verify these correction methods using a split-sample method, with one population of sea state statistics derived from observations to train the correction scaling, and another population of sea state statistics derived from measurements to validate it. Although model underbias is not observed to be affected by differences in regional wave climates, regional effects on scaling factors should not be ruled out and, therefore, should be investigated further.

The potential value of model bias correction for $H_{s(n)}$ is demonstrated for WEC design and wave energy resource assessment. Without correction, design load cases for extreme sea states, based on $H_{s(50)}$, and risks for wave energy projects, based on $H_{s(50)}$ and $H_{s(50)}/H_{s(mean)}$, would be significantly underestimated.

Acknowledgement

Sandia National Laboratories is a multi-mission laboratory managed and operated by National Technology and Engineering Solutions of Sandia, LLC., a wholly owned subsidiary of Honeywell International, Inc., for the U.S. Department of Energy's National Nuclear Security Administration under contract DE-NA0003525. This study was also partially funded by the U.S. Department of Energy, Office of Energy Efficiency & Renewable Energy, Water Power Technologies Office under Contract DE-AC05-76RL01830 to Pacific Northwest National Laboratory. This paper describes objective technical results and analysis. Any subjective views or opinions that might be expressed in the paper do not necessarily represent the views of the U.S. Department of Energy or the United States Government.

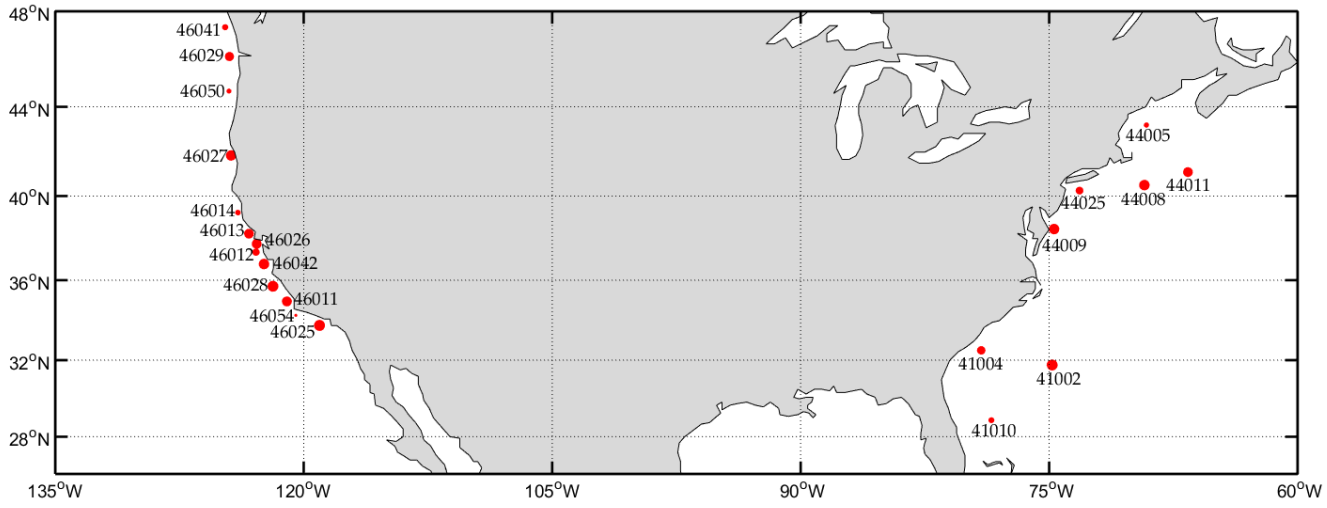

Fig. 1. NDBC buoy sites along US East and West Coasts selected for model performance study. The size of the circle indicates the period of record with smallest indicating 11 years (46054), and largest reflecting 22 years (e.g., 44008).

TABLE I
STUDY SITES AND COMPARISON OF 50-YEAR RETURN SIGNIFICANT WAVE HEIGHT

Station	POR (yrs.)	Depth (m)	Lat. (°)	Long. (°)	$H_{s(50)}$ (m)				
					Buoy	WWIII		SWAN	
						Raw	Corrected	Raw	Corrected
41002	20.97	4048	31.754	74.816	13.93	10.76 (-22.8%)	14.05 (0.9%)	13.52 (-3%)	14.63 (5%)
41004	12.54	39	32.501	79.099	10.01	7.88 (-21.3%)	10.29 (2.9%)	10.1 (0.9%)	10.92 (9.1%)
41010	12.84	890	28.878	78.485	10.69	8.79 (-17.8%)	11.48 (7.4%)	10.4 (-2.6%)	11.25 (5.3%)
44005	21.82	180.7	43.201	69.128	10.69	7.97 (-25.5%)	10.41 (-2.6%)	9.8 (-8.3%)	10.6 (-0.8%)
44008	21.98	74.7	40.504	69.248	12.31	9.31 (-24.4%)	12.16 (-1.3%)	10.55 (-14.3%)	11.42 (-7.3%)
44009	19.26	30	38.457	74.702	8.79	6.43 (-26.8%)	8.40 (-4.4%)	7.7 (-12.3%)	8.33 (-5.2%)
44011	19.60	82.9	41.098	66.619	15.02	11.79 (-21.5%)	15.40 (2.5%)	13.9 (-7.4%)	15.04 (0.1%)
44025	15.22	36.3	40.251	73.164	9.05	6.82 (-24.7%)	8.91 (-1.6%)	7.77 (-14.2%)	8.4 (-7.2%)
46011	19.31	464.8	34.956	121.019	10.62	8.3 (-21.8%)	10.85 (2.2%)	9.8 (-7.7%)	10.6 (-0.1%)
46012	19.61	208.8	37.356	122.881	10.34	8.57 (-17.1%)	11.19 (8.2%)	10.11 (-2.2%)	10.94 (5.8%)
46013	20.84	122.5	38.238	123.307	10.74	8.27 (-23%)	10.8 (0.6%)	9.49 (-11.6%)	10.27 (-4.4%)
46014	21.65	356	39.231	123.974	12.44	9.26 (-25.5%)	12.1 (-2.7%)	11.16 (-10.3%)	12.07 (-2.9%)
46025	20.87	888	33.761	119.049	6.89	5.39 (-21.8%)	7.04 (2.2%)	5.9 (-14.4%)	6.38 (-7.4%)
46026	20.71	54.9	37.754	122.839	9.42	6.81 (-27.7%)	8.90 (-5.6%)	10.95 (16.2%)	11.85 (25.7%)
46027	15.73	46.3	41.85	124.386	12.94	10.97 (-15.2%)	14.33 (10.7%)	12.09 (-6.6%)	13.08 (1%)
46028	18.21	1048	35.703	121.857	11.36	8.47 (-25.5%)	11.07 (-2.6%)	9.9 (-12.8%)	10.71 (-5.8%)
46029	13.51	134	46.143	124.485	14.16	11.56 (-18.4%)	15.10 (6.7%)	13.95 (-1.4%)	15.09 (6.6%)
46041	13.28	128	47.353	124.742	12.33	9.62 (-22%)	12.57 (1.9%)	11.2 (-9.2%)	12.12 (-1.7%)
46042	16.94	1645.9	36.785	122.398	11.40	8.6 (-24.5%)	11.24 (-1.4%)	9.84 (-13.7%)	10.64 (-6.7%)
46050	12.21	140	44.677	124.515	15.12	10.04 (-33.6%)	13.13 (-13.2%)	12.25 (-19%)	13.25 (12.4%)
46054	10.62	469.4	34.265	120.477	9.70	7.05 (-27.29%)	9.21 (-5%)	10.57 (9%)	11.44 (18%)
					B	23.2%	4.1%	9.4%	6.6%

The values in parentheses for Tables I-III indicate the percent difference between the model hindcast derived value and the buoy measurement derived value. This percent relative difference is calculated as $100 \cdot \left[\left(Mod.H_{s(50)} - Obs.H_{s\,(50)}\right)/Obs.H_{s\,(50)}\right]$. Note that the mean relative absolute bias, B, is the simple average of the absolute values of these relative differences.

TABLE II
STUDY SITES AND COMPARISON OF 5-YEAR RETURN SIGNIFICANT WAVE HEIGHT

Station	POR (yrs.)	Depth (m)	Lat. (°)	Long. (°)	$H_{s(5)}$ (m)				
					Buoy	WWIII		SWAN	
						Uncorrected	Corrected	Uncorrected	Corrected
41002	20.97	4048	31.754	74.816	10.03	7.91 (-21.1%)	9.84 (-1.8%)	9.5 (-5.2%)	10.28 (2.6%)
41004	12.54	39	32.501	79.099	7.4	6.01 (-18.7%)	7.48 (1.1%)	6.96 (-5.9%)	7.53 (1.8%)
41010	12.84	890	28.878	78.485	7.64	6.34 (-16.9%)	7.89 (3.4%)	7.3 (-4.4%)	7.9 (3.4%)
44005	21.82	180.7	43.201	69.128	8.27	6.4 (-22.7%)	7.96 (-3.8%)	7.47 (-9.7%)	8.09 (-2.3%)
44008	21.98	74.7	40.504	69.248	9.38	7.32 (-22%)	9.11 (-2.9%)	8.17 (-13%)	8.84 (-5.8%)
44009	19.26	30	38.457	74.702	6.61	5.95 (-9.9%)	7.4 (12.1%)	5.09 (-23%)	5.51 (-16.7%)
44011	19.60	82.9	41.098	66.619	10.6	8.35 (-21.2%)	10.39 (-2%)	9.52 (-10.2%)	10.3 (-2.8%)
44025	15.22	36.3	40.251	73.164	6.91	5.55 (-19.7%)	6.9 (-0.1%)	6.13 (-11.2%)	6.64 (-4%)
46011	19.31	464.8	34.956	121.019	7.77	6.18 (-20.4%)	7.69 (-1%)	7.13 (8.2%)	7.72 (-0.6%)
46012	19.61	208.8	37.356	122.881	7.83	6.7 (-14.4%)	8.34 (6.6%)	7.66 (-2.2%)	8.29 (5.9%)
46013	20.84	122.5	38.238	123.307	8.26	6.62 (-19.9%)	8.23 (-0.4%)	7.37 (-10.8%)	7.97 (-3.5%)
46014	21.65	356	39.231	123.974	9.39	7.34 (-21.8%)	9.13 (-2.7%)	8.53 (-9.2%)	9.23 (-1.7%)
46025	20.87	888	33.761	119.049	5.11	4.06 (-20.5%)	5.05 (-1.1%)	4.42 (-13.5%)	4.78 (-6.4%)
46026	20.71	54.9	37.754	122.839	6.93	5.5 (-20.5%)	6.85 (-1.1%)	8.42 (21.6%)	9.11 (31.6%)
46027	15.73	46.3	41.85	124.386	9.21	7.74 (-16%)	9.62 (4.5%)	8.57 (-7%)	9.27 (0.7%)
46028	18.21	1048	35.703	121.857	8.52	6.6 (-22.5%)	8.21 (-3.6%)	7.47 (-12.4%)	8.08 (-5.2%)
46029	13.51	134	46.143	124.485	10.35	8.82 (-14.8%)	10.97 (6%)	10.26 (-0.8%)	11.1 (7.3%)
46041	13.28	128	47.353	124.742	9.7	8.14 (-16%)	10.13 (4.5%)	9.22 (-4.9%)	9.98 (2.9%)
46042	16.94	1645.9	36.785	122.398	8.49	6.67 (-21.5%)	8.3 (-2.3%)	7.47 (-12%)	8.09 (-4.8%)
46050	12.21	140	44.677	124.515	11.17	8.34 (-25.4%)	10.37 (-7.1%)	9.73 (-12.9%)	10.52 (-5.8%)
46054	10.62	469.4	34.265	120.477	7.4	5.7 (-23%)	7.09 (-4.2%)	8.3 (12%)	8.98 (21.4%)
					B	19.5%	3.4%	10%	6.5%

TABLE III
STUDY SITES AND COMPARISON OF 1-YEAR RETURN SIGNIFICANT WAVE HEIGHT USING THE POT METHOD

Station	POR (yrs.)	Depth (m)	Lat. (°)	Long. (°)	$H_{s(1)}$ (m)				
					Buoy	WWIII		SWAN	
						Raw	Corrected	Raw	Corrected
41002	20.97	4048	31.754	74.816	7.88	6.25 (-20.7%)	7.75 (-1.7%)	6.99 (-11.3%)	7.66 (-2.9%)
41004	12.54	39	32.501	79.099	5.57	4.67 (-16.3%)	5.78 (3.8%)	5.07 (-9.1%)	5.55 (-0.4%)
41010	12.84	890	28.878	78.485	6.02	4.89 (-18.8%)	6.05 (0.6%)	5.47 (-9.2%)	5.99 (-0.5%)
44005	21.82	180.7	43.201	69.128	7.06	5.38 (-23.7%)	6.67 (-5.4%)	5.97 (-15.3%)	6.54 (-7.3%)
44008	21.98	74.7	40.504	69.248	7.81	6.21 (-20.6%)	7.69 (-1.6%)	6.89 (-11.8%)	7.55(-3.4%)
44009	19.26	30	38.457	74.702	5.42	4.32 (-20.2%)	5.36 (-1.2%)	4.98 (-8.2%)	5.45 (0.6%)
44011	19.60	82.9	41.098	66.619	8.62	6.62 (-23.2%)	8.21 (-4.8%)	7.3 (-15.3%)	8 (-7.2%)
44025	15.22	36.3	40.251	73.164	5.62	4.83 (-14%)	5.98 (6.5%)	5.1 (-9.2%)	5.59 (-0.5%)
46011	19.31	464.8	34.956	121.019	6.54	5.09 (-22.2%)	6.31 (-3.6%)	5.79 (-11.5%)	6.34 (-3.1%)
46012	19.61	208.8	37.356	122.881	6.54	5.63 (-13.9%)	6.97 (6.7%)	6.31 (-3.5%)	6.91 (5.7%)
46013	20.84	122.5	38.238	123.307	7.02	5.7 (-18.8%)	7.06 (0.6%)	6.16 (-12.2%)	6.75 (-3.9%)
46014	21.65	356	39.231	123.974	7.74	6.24 (-19.4%)	7.73 (-0.1%)	6.99 (-9.7%)	7.66 (-1.1%)
46025	20.87	888	33.761	119.049	4.08	3.25 (-20.4%)	4.03 (-1.4%)	3.56 (-12.9%)	3.9 (-4.6%)
46026	20.71	54.9	37.754	122.839	5.89	4.75 (-19.3%)	5.89 (0%)	6.97 (18.4%)	7.64 (29.6%)
46027	15.73	46.3	41.85	124.386	7.32	6.08 (-16.9%)	7.53 (2.9%)	6.61 (-9.7%)	7.24 (-1.1%)
46028	18.21	1048	35.703	121.857	7.1	5.47 (-22.9%)	6.78 (-4.5%)	6 (-15.4%)	6.58 (-7.4%)
46029	13.51	134	46.143	124.485	8.69	7.3 (-16%)	9.04 (4.1%)	8.25 (-5.1%)	9.03 (4%)
46041	13.28	128	47.353	124.742	8	7.13 (-10.8%)	8.84 (10.5%)	7.72 (-3.5%)	8.45 (5.7%)
46042	16.94	1645.9	36.785	122.398	6.95	5.53 (-20.5%)	6.85 (-1.5%)	6.07 (-12.7%)	6.65 (-4.3%)
46050	12.21	140	44.677	124.515	9.2	7.2 (-21.8%)	8.92 (-3.1%)	8 (-13.1%)	8.76 (-4.8%)
46054	10.62	469.4	34.265	120.477	6.31	4.92 (-22%)	6.1 (-3.4%)	6.95 (10.1%)	7.61 (20.6%)
					B	19.6%	3.2%	10.8%	5.7%

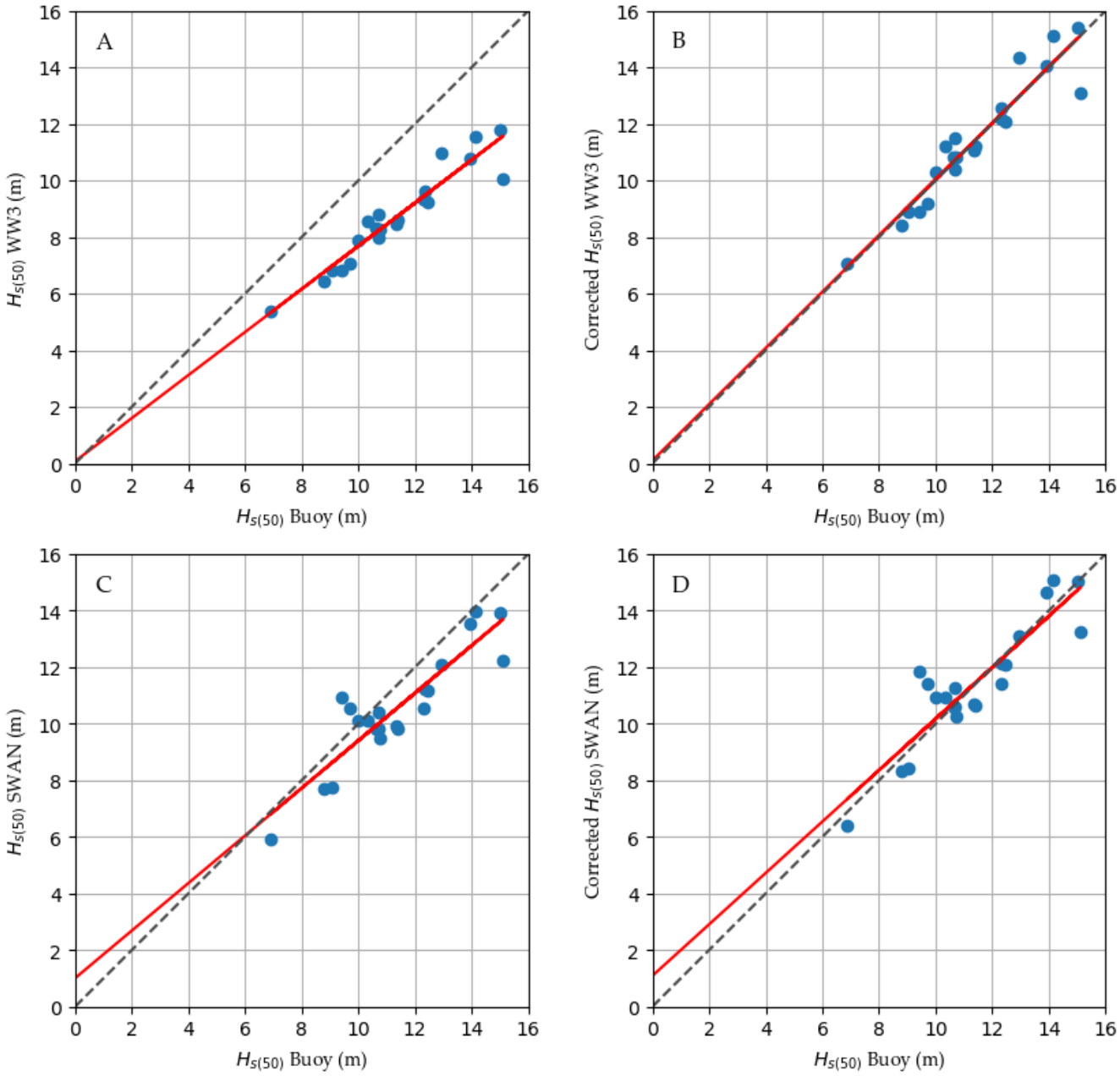

Fig. 2. Scatter plots at twenty-one NDBC stations comparing $H_{s(50)}$ derived from models with $H_{s(50)}$ derived from in situ observations at NDBC buoy stations. Dashed lines represent lines of equivalence. Red lines represent lines of best fit from linear regression. $H_{s(50)}$ are adjusted by linear scaling with scaling factor, s using (1): A, raw $H_{s(50)}$ WWIII hindcast vs. $H_{s(50)}$ buoy (regression r^2=0.90, m=0.76, b=0.08); B, corrected $H_{s(50)}$ WWIII hindcast vs. $H_{s(50)}$ buoy (s=1.31, regression r^2=0.90, m=0.99, b=0.11); C, raw $H_{s(50)}$ SWAN hindcast vs. $H_{s(50)}$ buoy (regression r^2=0.81, m=0.84, b=1.0); D, corrected $H_{s(50)}$ SWAN hindcast vs. $H_{s(50)}$ buoy (s=1.08, regression r^2=0.81, m=0.91, b=1.1).

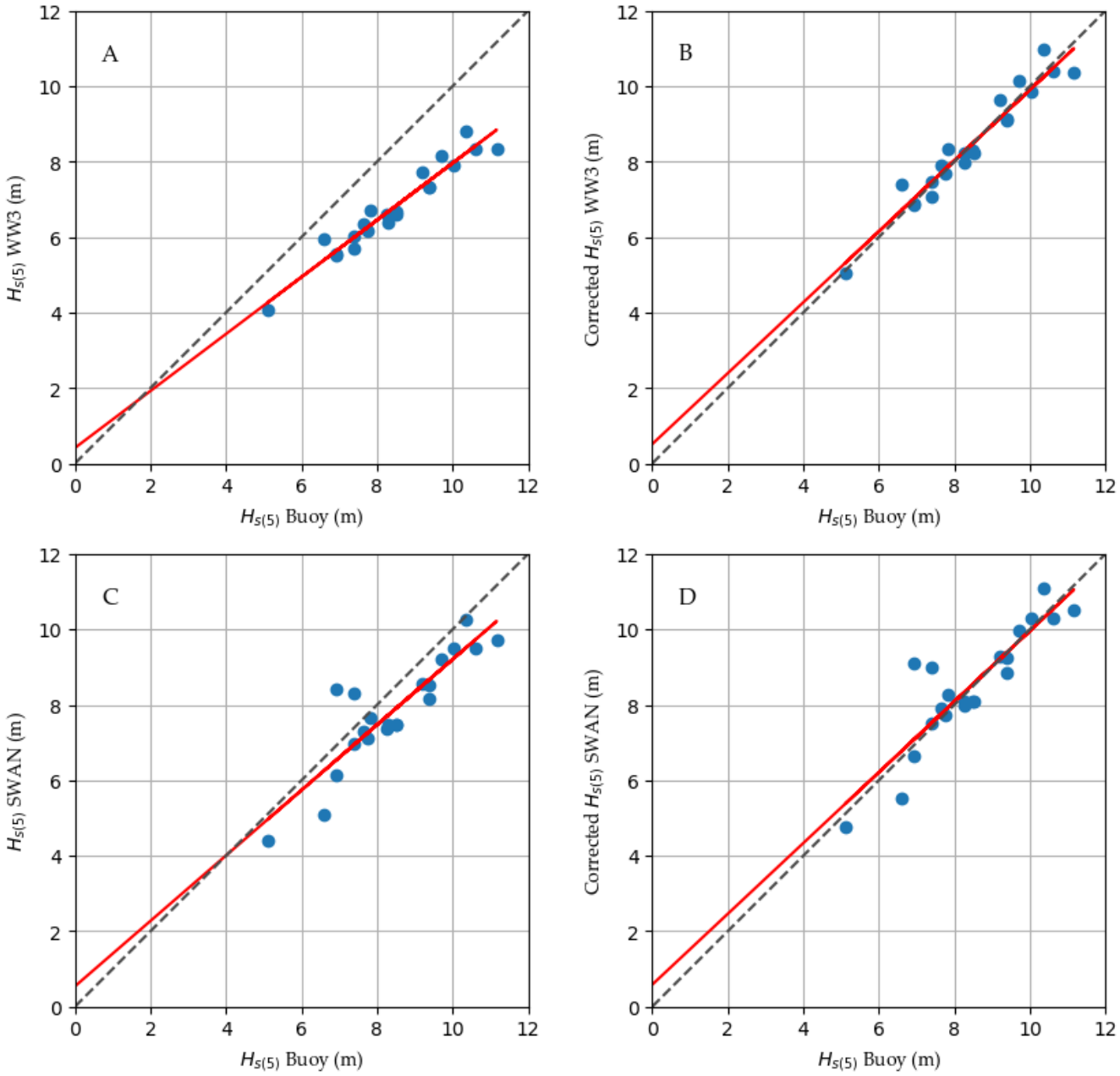

Fig. 3. Scatter plots at twenty-one NDBC stations comparing $H_{s(5)}$ derived from models with $H_{s(5)}$ derived from in situ observations at NDBC buoy stations. Dashed lines represent lines of equivalence. Red lines represent lines of best fit from linear regression. $H_{s(5)}$ are adjusted by linear scaling with scaling factor, s using (1): A, raw $H_{s(5)}$ WWIII hindcast vs. $H_{s(5)}$ buoy (regression r^2=0.94, m=0.755, b=0.413); B, corrected $H_{s(5)}$ WWIII hindcast vs. $H_{s(5)}$ buoy (s=1.24, regression r^2=0.94, m= 0.939, b= 0.513); C, raw $H_{s(5)}$ SWAN hindcast vs. $H_{s(5)}$ buoy (regression r^2=0.79, m=0.866, b=0.540); D, corrected $H_{s(5)}$ SWAN hindcast vs. $H_{s(5)}$ buoy (s=1.08, regression r^2=0.79, m=0.938, b=0.583).

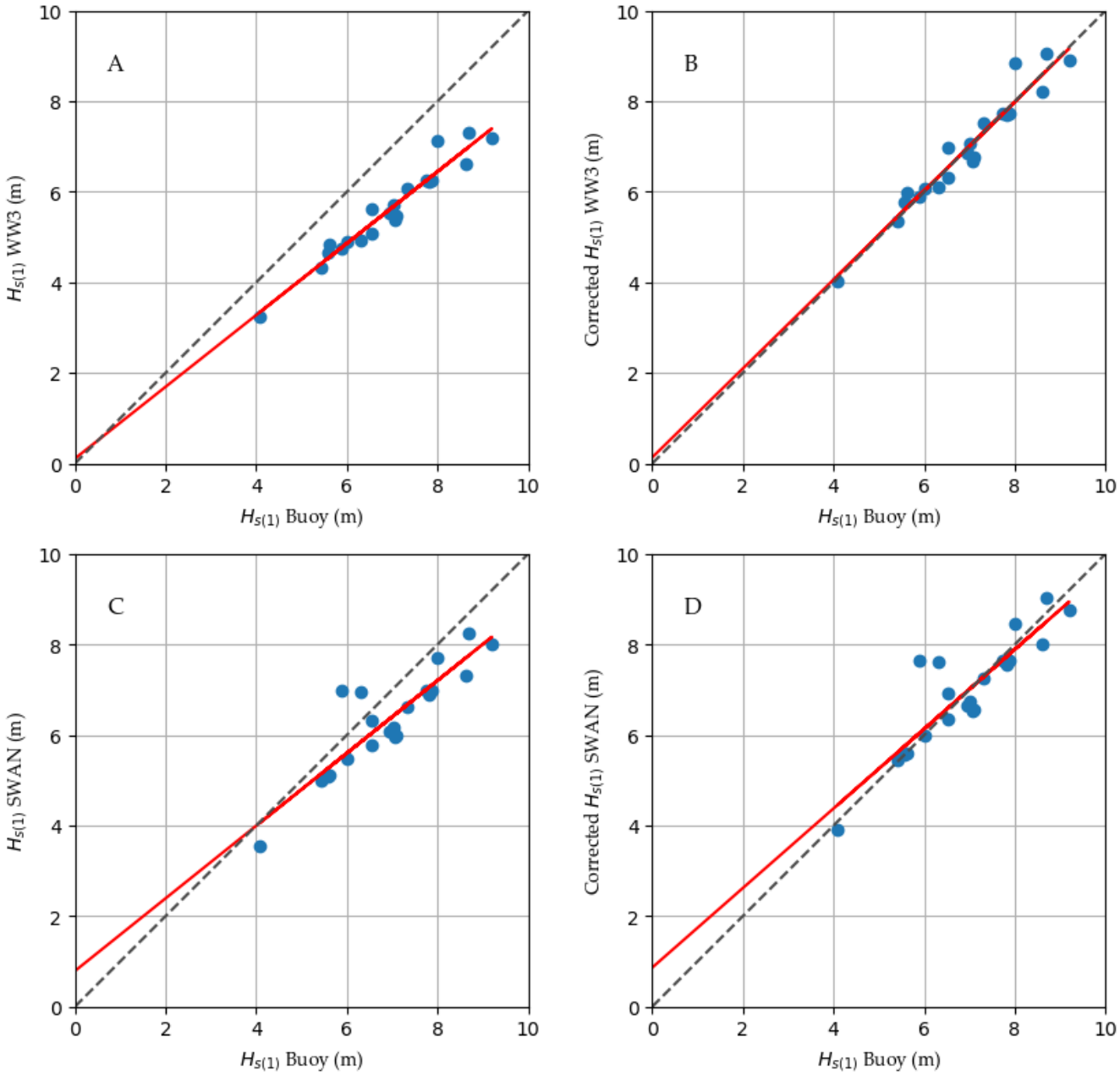

Fig. 4. Scatter plots at twenty-one NDBC stations comparing $H_{s(1)}$ derived using the MQQR POT method from models with $H_{s(1)}$ derived using the MQQR POT method from in situ observations at NDBC buoy stations. Dashed lines represent lines of equivalence. Red lines represent lines of best fit from linear regression. $H_{s(1)}$ are adjusted by linear scaling with scaling factor, s using (1): A, raw $H_{s(1)}$ WWIII hindcast vs $H_{s(1)}$ buoy (regression r^2=0.94, m=0.792, b=-0.111); B, corrected $H_{s(1)}$ WWIII hindcast vs. $H_{s(1)}$ buoy (s=1.24, regression r^2=0.94, m= 0.981, b=0.137); C, raw $H_{s(1)}$ SWAN hindcast vs. $H_{s(1)}$ buoy (regression r^2=0.80, m= 0.802, b=-0.790); D, corrected $H_{s(1)}$ SWAN hindcast vs. $H_{s(1)}$ buoy (s=1.10, regression r^2=0.80, m=0.878, b=0.865).

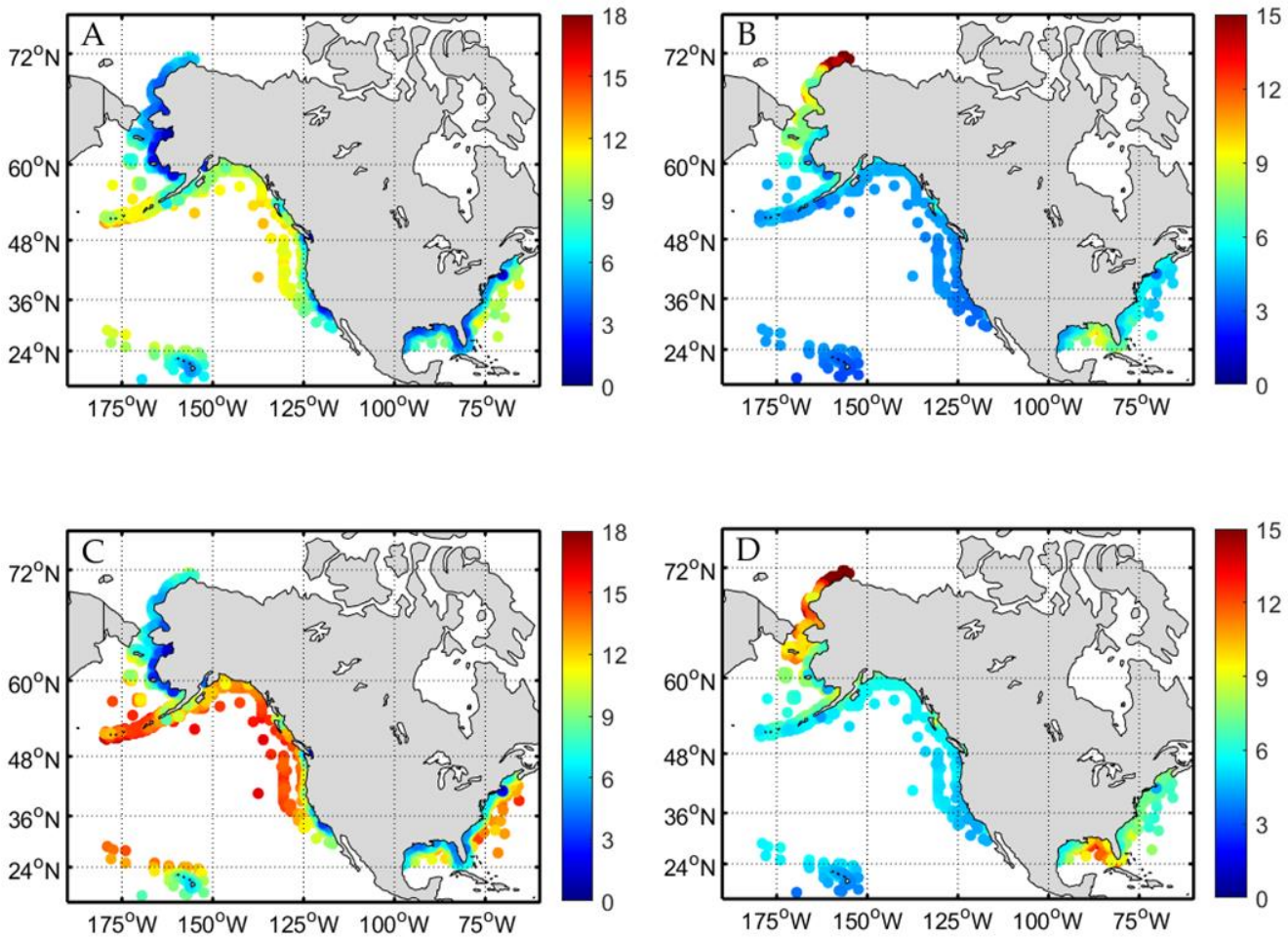

Fig. 5. Comparison of raw and corrected geo-spatial distribution of $H_{s(50)}$ and the relative risk ratio, $H_{s(50)}/H_{s(mean)}$ for 1,978 sites in US coastal waters generated from a 30-year WaveWatch III hindcast. : A, raw $H_{s(50)}$; B, raw $H_{s(50)}/H_{s(mean)}$; C, corrected $H_{s(50)}$ adjusted by the scaling factor, s =1.31 as noted in Fig. 2; D. corrected $H_{s(50)}/H_{s(mean)}$ adjusted by the scaling factor, s =1.31 as noted in Fig. 2. The color scale indicates the 50-year return significant wave height (m) for graphs A and C, and the relative risk ratio value for graphs B and D.

REFERENCES

[1] Y. Goda, Random Seas and Design of Maritime Structures Advanced Series on Ocean Engineering, vol. 33, World Scientific Publishing Ltd., 2010.

[2] G. Hagerman, "Oceanographic design criteria and site selection for ocean wave energy conversion," in *Proceedings IUTAM Symp. Hydrodynamics of Ocean Wave Energy Utilization, Lisbon*, Springer Verlag, 1985, pp. 937–942.

[3] V. S. Neary, R. G. Coe, J. Cruz, K. Haas, G. Bacelli, Y. Debruyne, S. Ahn, V. Nevarez, "Classification systems for wave energy resources and WEC technologies," *Int. Marine Energy Journal*, vol. 1, no. 2, pp. 71-79, 2018.

[4] Marine energy - Wave, tidal and other water current converters - Part 2: Design requirements for marine energy systems, IEC TS 62600-2:2016-08.

[5] L. R. Muir and A. H. El-Shaarawi. On the calculation of extreme wave heights: a review. *Ocean Engng*., vol. 13, no. 1, pp. 93-118, 1986.

[6] J. H. G. M. Alves, I. R. Young, "On estimating extreme wave heights using combined Geosat, Topex/Poseidon and ERS-1 altimeter data," Applied Ocean Research, vol. 25, pp. 167-186, 2003.

[7] Marine energy - Wave, tidal and other water current converters - Part 101: Wave energy resource assessment and characterization, IEC TS 62600-101:2015-06.

[8] Det Norske Veritas, Recommended Practice - Environmental conditions and environmental loads, DNV-RP-C205:2014.

[9] Z. Yang, V. S. Neary, T. Wang, B. Gunawan, A. R. Dallman, W. Wu, "A wave model test bed study for wave energy resource characterization," *Renew Energy*, vol. 114, pp. 132-144, 2017.

[10] Z. Yang, W. C. Wu, T. Wang, L Castrucci, "High Resolution Regional Wave Hindcast for the U.S. West Coast," PNNL Technical Report, PNNL-28107. Pacific Northwest National Laboratory, Richland, WA. 2018

[11] N. Allahdadi, B. Gunawan, J. Lai, R. He, V. S. Neary, "Development and validation of a regional-scale high resolution unstructured model for wave energy resource characterization," *Renew Energy*, vol. 136, pp. 500-511, 2019.

[12] X. L. L. Wang, V. R. Swail, "Changes of extreme wave heights in northern hemisphere oceans and related atmospheric circulation regimes, *J. Clim*. vol. 14, no. 10, pp. 2204-2221, 2001.

[13] T. Wang, Z. Yang, W. Wu, M. Gear, "A sensitivity analysis of the wind forcing effect on the accuracy of large-wave hindcasting," *J. Mar. Sci. Eng*., vol. 6, no. 139, pp. 1-15, 2018.

[14] S. A. Stephens, R. M. Gorman, "Extreme wave predictions around New Zealand from hindcast data," *New Zealand J. Mar. Fresh Res*., vol. 40, no. 3, pp. 399-411, 2006.

[15] J. L. Hanson, B. A. Tracy, H. L. Tolman, R. D. Scott, "Pacific hindcast performance of three numerical wave models," *J of Atm. Oc Tech*, vol. 26, pp. 1614-1633.

[16] A. Chawla, D. M. Spindler, H. L. Tolman, "Validation of a thirty-year wave hindcast using the Climate Forecast System Reanalysis winds," *Ocean Model*, vol. 70, pp. 189-206, 2013.

[17] Z. Yang, V. S. Neary, "U.S. regional wave model hindcasts for wave resource characterization, classification and assessment," European Wave and Tidal Energy Conference, 2019.

[18] B. E. Seng, V. S. Neary, "Extreme wave height estimation for energy resource classification," presented at the American Geophysical Union (AGU) Fall Meeting, 2018.